Development of Microbeam Scanning System

V. 3. Development of Microbeam Scanning System

Oyama R.[1], Matsuyama S.[1], Ishii K.[1], Yamazaki H.[2], Kikuchi Y.[1], Inomata K.[1], Watanabe Y.[1], Ishizaki A.[1], Kawamura Y.[1], Yamaguchi.[1], and Momose G.[1]

[1]Department of Quantum Science and Energy Engineering, Tohoku University,
[2]Cyclotron and Radioisotope Center, Tohoku University

Introduction

High-energy ion microbeams are powerful analytical tools when used in combination with various ion beam analysis techniques; they are also attractive as a direct micro fabrication technique[1-3]. We have developed a microbeam scanning system that is suitable for these purposes. In microbeam analysis systems, microbeams are scanned over a square region of sample. However, analysis samples, such as cultured single cells or collected aerosol particles are not always distributed all over. In such cases, irradiation on areas where specimens are not distributed merely prolongs the analysis time. In micro fabrication, such as proton beam writing (PBW), the situation is rather essential. Microbeams are scanned on the sample and are kicked away where irradiation is not needed. Irradiation time would be shortened if microbeams were scanned with a pattern corresponding to the sample area or processing pattern. As described herein, we developed a microbeam scanning system that is suitable for efficient analysis and for micro fabrication such as PBW.

Beam scanning system

The microbeam system was designed and then developed to achieve sub-micrometer beam sizes[4-7]. The microbeam system comprises a quadrupole doublet and three slit systems. The scanner is located ca. 8 cm downstream of the quadrupole doublet. The scanning system comprises a set of electrostatic deflectors, high-voltage (HV) amplifiers, buffer amplifiers, and a function generator. A schematic diagram of the scanning system and data acquisition system is shown in Fig. 1. The data acquisition system of multimodal analysis was described precisely in previous papers[1].

The electrostatic deflector was 25 mm long and 16 mm wide, with 3 mm spacing. Both ends of the deflector plate along the longitudinal direction, the beam direction, have steps of 0.5 mm to reduce the fringing field effect. Each deflector was driven by an independent HV amplifier to obtain a uniform and symmetric electrostatic field. In total four HV amplifiers were used in the system for horizontal and vertical scanning. In the original design, the deflector was 25 mm long and 16 mm wide, with 5 mm spacing and without steps at both ends. One of the deflector plates was driven by an HV amplifier and the other deflector plate was grounded. Two amplifiers were used for horizontal and vertical scanning, respectively.

Figure 2 shows elemental images of Cu mesh (100 lines/inch) for a scanning area of 350×450 μm^2 measured with the two HV amplifier system (left) and with the four HV amplifier system (right). Both images were obtained in the same beam condition with the same deflectors of 25 mm long and 16 mm wide, with 5 mm spacing. The mesh image obtained by using the two amplifier system is not clearly seen in the upper left and the lower right regions. On the other hand, using the four amplifier system, the image is clearly seen over the scanning area. Thus, the four HV amplifier system is indispensable to obtain the same beam spot size at any scanning position.

Figure 3 shows the mesh images obtained with the no step deflectors (left) and with the stepped deflectors (right), respectively. These deflectors were driven by the four HV amplifiers. The images were compared for elemental images of Au and Ni mesh (2000 lines/inch), respectively, with five scanning areas of 30×30 μm^2 at the center position, and at the four corners of the 600×600 μm square. Beam conditions are almost same in both measurements. The images obtained using the no step deflectors are deformed at the corners of the 600×600 μm square, especially at the upper left and the lower right areas. On the other hand, the images measured with the stepped deflectors show the same quality with no deformation at any position. Therefore, the four HV amplifier system and deflector shape which reduces the fringing field effect are indispensable to keep the beam spot size at any scanning position.

The HV amplifier (HOPS1.5B2; Matsusada Precision Inc.) is a fast response HV bipolar amplifier with a slew rate of 12 V/μs. The maximum voltage is 1.5 kV. Therefore, the obtained electrostatic field of 1 kV/mm is sufficient to shift the 3 MeV proton beam to more than 0.5 mm on the target position. The amplifier amplifies a -10 to 10 V signal into a -1.5 to +1.5 kV signal. A four-channel function generator of a PC-based measurement

instrument (WE-7282; Yokogawa Electric Corp.) is used for X-Y beam scanning and for elemental imaging. Two channels out of four were used as scanning signals to drive the HV amplifiers for the scanners. Other two are used as X-Y position signals corresponding to the beam scanning. Each beam scanning signal is divided into two signals and is introduced into the buffer amplifier. One is inverted; the other is not inverted. While raster scanning is utilized in the conventional analysis, the beam can be scanned according to an arbitrary pattern. Varying the irradiation time alters the irradiation dose. The function generator can output 10^6 points of DC voltage sequentially even in the minimum time scale of 10 μs/point, so as to generate complicated voltage patterns in a short period. Thus the microbeams can be just scanned with a corresponding pattern of the analyzing sample area or of the fabrication form. Between the patterns, the beams are moved with the fastest responsive scan speed. We call the process as the pattern-to-pattern spacing procedure.

The scanning speed is also an important factor. The beam scanning speed must be high to keep correct irradiation dose on the pattern and to reduce the irradiation dose between pattern-to-pattern spacing. Measurements of the beam scanning speed versus the beam spot size were carried out by scanning the beam one-dimensionally on the Ni mesh (2000 lines/inch). The beam was scanned on a line of 150 μm length with the scanning speeds ranging from 0.3 to 60 mm/s. The X-ray yield profile was fitted using symmetric double-Gaussian convolution and the beam spot size was obtained. The yield profiles at scanning speeds of less than 9 mm/s show a similar shape, although they are deformed and finally split into two peaks at the speed of 60 mm/s, especially on both sides. This is due to deformation of the output of the HV amplifier at the tops and bottoms of the triangular waveform, that is, the HV amplifier is unresponsive to sudden changes of voltage and thus, waveform was deformed. Therefore, the maximum scanning speed can be estimated at 9 mm/s to keep correct irradiation dose on the irradiation pattern.

Application to the microbeam analyses

Microbeam analysis samples, such as cultured single cells or collected aerosol particles are not always distributed all over. Figure 4 shows a microphotograph of cells cultured on the polycarbonate film. In this case, cells occupy only half of the scanning area. The analysis time is reduced greatly if the beams are scanned only on the cells. In order to define the regions of the cells, scanning transmission ion microscopy (STIM) mapping was used. This is very useful to achieve structural and density imaging for the

scanning area in a short period, because in STIM, transmitted ions are detected with almost 100 % efficiency[1]. Figure 5 shows a STIM map of the cells according to the area shown in Fig. 4. Cells are clearly apparent in the map and correspond to the microphotograph. While application of optical images obtained using a microscope is also applicable for this system, position calibration is not easy. In case of STIM imaging, position calibration is not needed. The scanning pattern, which corresponded to the areas of the cells, was translated from the STIM map. Transmitted ion energies vary corresponding to the cell thickness. Therefore, appropriate transmitted ion energy range has to be selected to define the areas of the cells properly. To cover all the cell areas, transmitted ion energy range was selected widely considering the energy resolution of the charged particle detector. Using the STIM-based scanning pattern, microbeams can be made to irradiate only the cells. In order to check the scanning pattern and the dose in the irradiation area, before cell analysis using the STIM-based scanning pattern, titanium foil of 0.2 μm thick was irradiated with this pattern and an X-ray yield map was obtained. The X-ray map is shown in Fig. 6 along with the irradiation pattern obtained from the STIM map and with the relative X-ray yield per square micrometer in the indicated areas. Total irradiation points were 263,168 points; 263 s are required for one scan. The scan was repeated until an X-ray yield reached a predetermined yield. The beams were scanned with the settled pattern as shown in fig 6. The X-ray yield is constant, as shown in Fig. 6. Fluctuation of the beam current was averaged by repeated beam scanning.

Then the cells were analyzed using the STIM-based scanning and with the conventional raster scanning. Figure 7 shows elemental concentration maps of cells with the STIM-based scanning and the conventional scanning. The total accumulated charges were around 170 nC for both measurements. X-rays were detected only from the settled patterns. However, in the space between the cells, there are fractions of patterns, and X-rays were partly detected. Since the range of the transmitted ion energy was set widely to cover all the cell area, some of the areas where cells were not distributed was recognized as the areas of cells and were irradiated.

Elemental concentrations in the cell derived from these scanning methods mutually coincide within statistical error. Statistical errors in the STIM-based scanning are better than those in the raster scanning in the cell regions because STIM-based scanning increases the irradiation dose in the cell area. In case of the same statistical error, the irradiation time is reducible to 1/2.5 with the same statistical error. Consequently, the STIM-based scanning system reduces the necessary analysis time, as shown in the actual sample

analysis.

Application to proton beam writing

Proton beam writing was achieved by scanning the microbeam with a corresponding scanning pattern translated from a bitmap file. The irradiation dose corresponds to the color and is changed by varying the irradiation time. Several patterns translated from bitmap files were inscribed on Mylar and polyester films to demonstrate the performance of the scanning system. The thickness of the Mylar and polyester films were 100 and 100 μm, respectively. RBS analysis was performed to monitor the irradiation dose. After the irradiation of the Mylar film, direct STIM analysis was carried out. Figure 8 shows a microphotograph, an RBS map, and direct STIM images of a Mylar film after irradiation with a scanning pattern of Chinese characters: 小山 亮平. The irradiation pattern is clearly apparent both on the microphotograph and on the direct STIM image. The RBS image also shows that irradiation was made solely on the character. The beam spot sizes of 0.7×0.9 μm^2 with a beam current of 50 pA is used in this irradiation. The total accumulated charge was 260 nC. Figure 9 shows STIM spectra for i (irradiation area), ii (space between irradiation area), and iii (non-irradiation area). In region i, the elemental loss occurred and the transmitted energy was increased. In the regions of ii and iii, no difference was found. Irradiation damage was not measurable in the space between irradiation areas; for that reason, the fast beam skip is useful for PBW. A design of a Japanese classical toy was inscribed on a polyester film of 100 μm. A micrograph and RBS map are shown in Fig. 10. The irradiation was made using a beam spot size of 1.0×1.5 μm^2 with a beam current of 300 pA. This design was inscribed with two tones and is shown in the RBS map. The lower irradiation dose was 40 pC/μm^2; the higher one was 200 pC/μm^2. Red coloration corresponding to the irradiation dose was clearly apparent. A red shift occurred in the irradiation area[1)].

Conclusions

We developed a new microbeam scanning system that is suitable for microbeam analyses and PBW. The system accomplished a pattern-to-pattern spacing procedure, in which the microbeam was just scanned with a corresponding pattern of the analyzing sample area or of the fabrication form. Between the patterns, the beam was moved with the fastest responsive scanning speed. For efficient analysis, a STIM image was translated

into a scanning pattern. As the result, analyzing time was greatly reduced for the cell sample in which cells are not distributed all over. The scanning system was also applied to PBW. Where a pattern was translated from bitmap data including color scale, which was translated to the irradiation time in proportion to the irradiation dose. Several patterns were inscribed on thin polymer foils as demonstrations. The scanning system will be useful for efficient analysis and PBW.

Acknowledgements

This study was partly supported by Grants-in-Aid for Scientific Research (S) from the Ministry of Education, Culture, Sports, Science and Technology, Japan: No. 13852017, (B) No. 18360450, and (C) No. 16560731. The authors gratefully acknowledge the assistance of R. Sakamoto and M. Fujisawa for maintenance and operation of the Dynamitron accelerator. The authors would also like to thank Messrs. K. Komatsu, T. Nagaya and C. Akama for their assistance in constructing the microbeam system.

References

1) Watt F., Grime G.W., Principal and Applications of High-energy Ion Microbeams, Adam Hilger, Bristol, 1987.
2) Johansson S.A.E., Campbell J.L., Malmqvist K.G., Particle-Induced X-ray Emission Spectrometry (PIXE), John Wiley and Sons, N.Y., 1995.
3) Breese M.B.H., Jamieson D.N., King P.J.C., Materials Analysis using Nuclear Microprobe, John Wiley and Sons, N.Y., 1995.
4) Matsuyama S., Ishii K., Yamazaki H., Sakamoto R., Fujisawa M., Amartaivan Ts., Ohishi Y., M Rodriguez., Suzuki A., Kamiya T., Oikawa M., Arakawa K., Matsumoto N., Nucl. Instr. Meth., **B210** (2003) 59.
5) Matsuyama S., Ishii K., Yamazaki H., Y Barbotteau., Amartivan Ts., Izukawa D., Hotta K., Mizuma K., Abe S., Oishi Y., M Rodriguez., Suzuki A., Sakamoto R., Fujisawa M., Kamiya T., Oikawa M., Arakawa K., Imaseki H., Matsumoto N., Int. J. PIXE, **14** (2004) 1.
6) Matsuyama S., Ishii K., Yamazaki H., Kikuchi Y., Inomata K., Watanabe Y., Ishizaki A., Oyama R., Kawamura Y., Yamaguchi T., Momose G., Nagakura M., Takahashi M., Kamiya T., Nucl. Instr. Meth. **B260** (2007) 55.
7) Matsuyama S., Ishii K., Yamazaki H., Kikuchi Y., Amartivan Ts., Abe S., Inomata K., Watanabe, A.Ishizaki Y., Oyama R., Kawamura Y., Suzuki A., Momose G., Yamaguchi T., Imaseki H., Int. J. PIXE, **15** (2005) 257.
8) Matsuyama S., Ishii K., Sugimoto A., Satoh T., Gotoh K., Yamazaki H., Iwasaki S., Murozono K., Inoue J., Hamano T., Yokota S., Sakai T., Kamiya T., Tanaka R., Int. J. PIXE, **8** (1998) 203.
9) Inomata K., Ishii K., Yamazaki H., Matsuyama S., Kikuchi Y., Watanabe Y., Ishizaki A., Oyama R., Kawamura Y., Yamaguchi T., Momose G., Sakurai E., Yanai K., Kamiya T., Sakai T., Satoh T., Oikawa M., Arakawa K., Int. J. PIXE, **16** (2006) 149.
10) Matsuyama S., Ishii K., Yamazaki H., Endoh H., Yuki H., Sato T., Sugihara S., Amartaivan Ts., Tanaka A., Komori H., Orihara H., Int. J. PIXE, **11** (2001) 93.

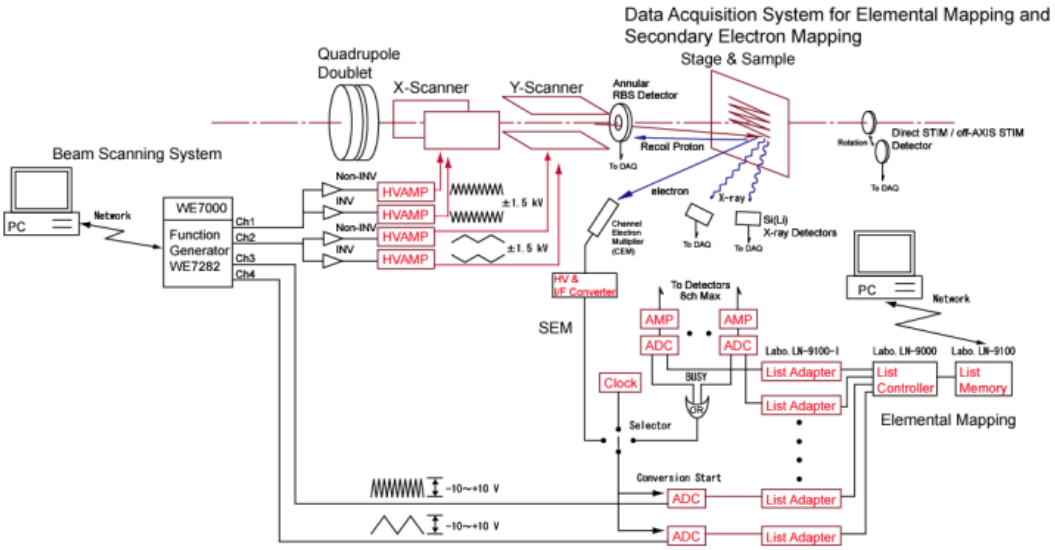

Figure 1. Schematic diagram of the beam scanning system and data acquisition system.

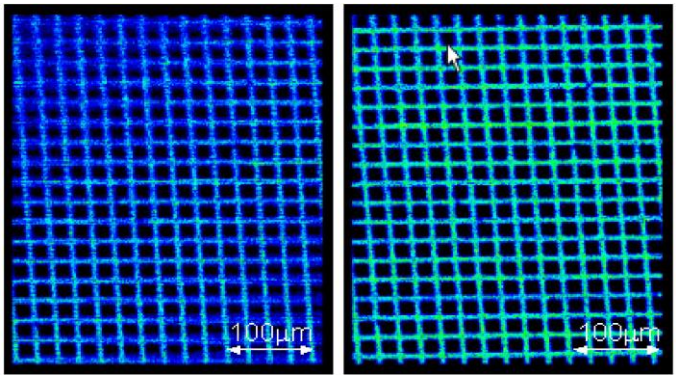

Figure 2. Elemental images of Cu mesh (1000 lines/inch) for a scanning area of 350 ×450 μm with the two HV amplifier system(left) and with the four amplifier system.

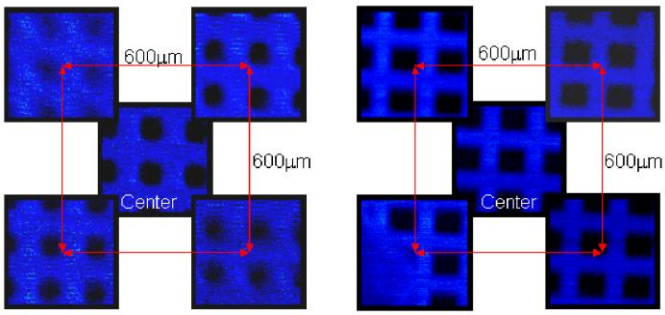

Figure 3. Elemental images of Au (left) and Ni (right) mesh (2000 lines/inch) with five scanning areas of 30×30 μm^2 at the center position, and at the four corners of the 600×600 μm square measured with the no step deflectors (left) and the stepped deflectors (right).

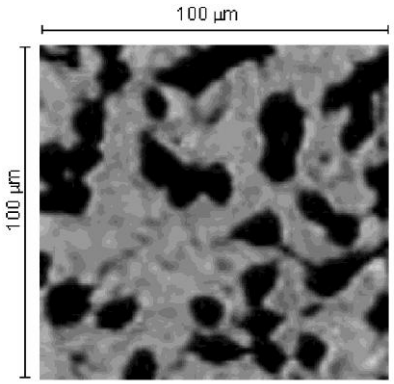

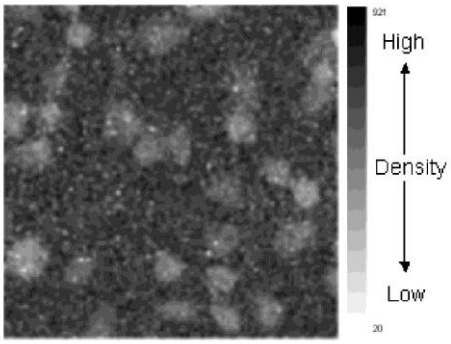

Figure 4. Microphotograph of Cultured Cells. Figure 5. STIM Map of Cultured Cells.

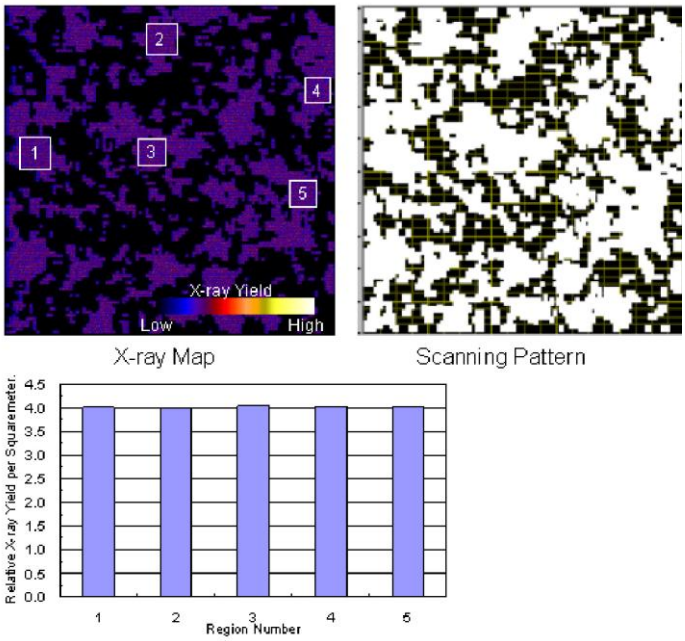

Figure 6. X-ray yield from titanium foil with STIM-based scanning, irradiation pattern and X-ray yields from the indicated areas.

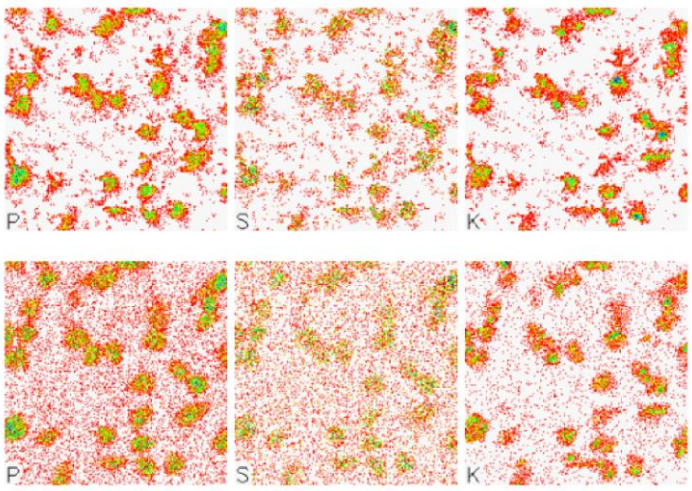

Figure 7. Elemental concentration maps of cells with the STIM-based scanning (upper) and conventional scanning (lower).

Figure 8. Microphotograph, RBS Map, and Direct STIM Images of a Mylar film after Irradiation with a Scanning Pattern of Chinese Characters: 小山 亮平.

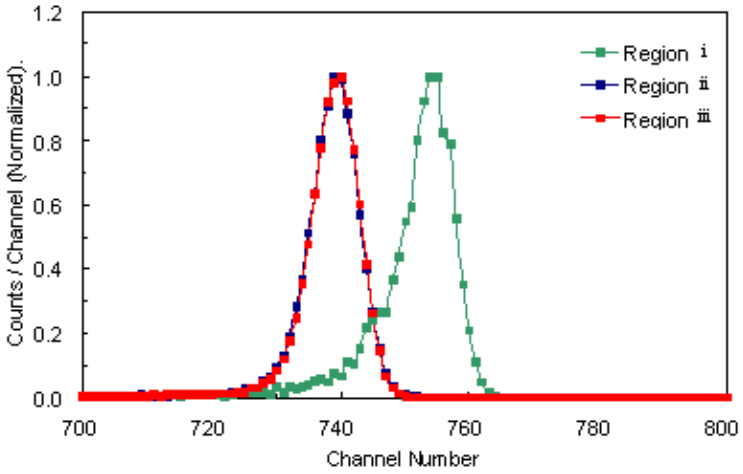

Figure 9. STIM spectra for Regions i (irradiation area), ii (space between irradiation area), and iii (non-irradiation area) in Fig. 7.

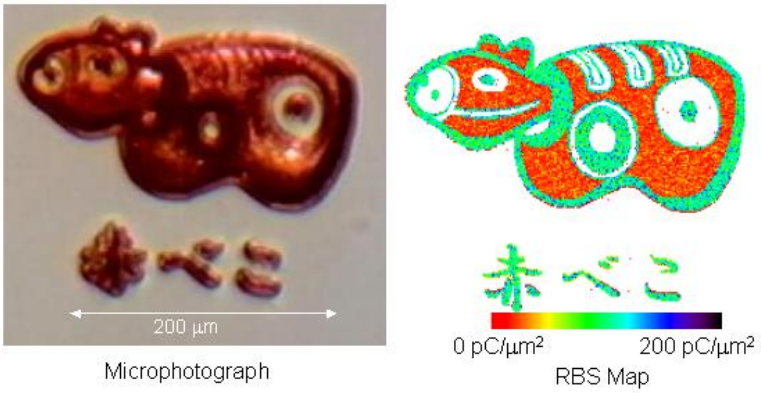

Figure 10. Design of a Japanese Classical Toy Inscribed on the Polyester Film and RBS.